

# Cavity-soliton laser with frequency-selective feedback

A. J. Scroggie,<sup>\*</sup> W. J. Firth, and G.-L. Oppo*Department of Physics, University of Strathclyde, 107 Rottenrow, Glasgow G4 0NG, Scotland, United Kingdom*

(Received 26 November 2008; published 28 July 2009)

We present a coupled-cavity model of a laser with frequency-selective feedback, and use it to analyze and explain the existence of stationary and dynamic spatial solitons in the device. Particular features of soliton addressing in this system are discussed. We demonstrate the advantages of our model with respect to the common Lang-Kobayashi approximation.

DOI: [10.1103/PhysRevA.80.013829](https://doi.org/10.1103/PhysRevA.80.013829)

PACS number(s): 42.60.Mi, 42.65.Tg, 05.45.Yv

## I. INTRODUCTION

The study of self-localized beams of light in dissipative (cavity) optical systems is now well-developed and encompasses a range of materials and devices (see [1]). Examples of systems which support such cavity solitons (CS) include Kerr [2] and absorptive [3,4] cavities, optical parametric oscillators [5], and semiconductor amplifiers [6,7]. In these cases a driving field is needed in order to sustain excitation in the lossy cavity. Use of such a holding beam has the benefit of allowing relatively straightforward control of CS motion and position through phase and amplitude gradients [3,8,9]. However, it comes at the cost of maintaining a broad-area coherent beam across the transverse extent of the device.

A cavity soliton laser, on the other hand, would have the advantage of requiring only incoherent pumping, which need not even be optical. It would exhibit lasing in a narrow self-localized beam, or (reconfigurable) ensemble of beams, from a spatially extended pump. Unfortunately, localized lasing on a stable dark background requires bistability between two states and this is not present in the standard laser. Lasers with injected signal are known to be capable of supporting CS [10,11] but these bear more resemblance to passive systems, requiring a coherent holding beam to which the CS is frequency locked.

One promising solution is to add a saturable absorber to the laser cavity [12,13] or to use coupled lasing and absorbing vertical cavity surface emitting lasers (VCSELs) [14] in order to create bistability, but at the cost of increased losses and the complication of a second nonlinear element. In contrast, a recently demonstrated alternative [15,16] uses frequency-dependent feedback to selectively *lower* the system losses and in a way that is entirely linear in the optical field.

Purely temporal effects in the dynamics of lasers with optically filtered feedbacks have been studied for some time [17]. Recently spatially localized structures have been described in the single-pass-feedback approximation [18,19]. Here we present a theoretical description and analysis of the spatiotemporal dynamics of a laser with intracavity frequency-selective feedback. We describe the mechanism for lasing and explore the system's ability to sustain both stationary and dynamic spatial solitons.

In Sec. II we introduce our theoretical description of the laser with frequency-selective feedback (FSF). Section III uses traveling-wave modes as a basis for describing the general behavior of the system. Since high reflectivities of the feedback mirror are an experimental requirement of the described CS lasers, in Sec. IV we point out the advantages of our model over more familiar theoretical approaches to lasers with feedback [17–23]. Section V analyzes single-frequency solitons, the basic building blocks of our understanding of the system. Section VI discusses features of soliton addressing in the laser and provides a qualitative guide and comparison for experiment. Finally, Sec. VII treats more complicated multifrequency soliton behavior. We end with conclusions and an outlook on the advantages of FSF with respect to other proposed CS lasers.

## II. MODEL

Our system consists of a VCSEL coupled to an external cavity which is formed by the addition of an external Bragg reflector (Fig. 1). The Bragg reflector provides frequency-selective feedback, lowering the laser threshold but only in a narrow frequency range around the peak of the Bragg reflection. Far from this frequency the feedback is negligible, as most light is transmitted by the grating. A lot of work has been devoted to the description of the temporal dynamics of semiconductor lasers with optical feedback (see, for example, [17,23]). The experimental setup of the cavity soliton laser of Fig. 1 [15,16], however, requires the inclusion of the transverse-space degrees of freedom, diffraction, and high reflectivity of the feedback mirror. The coupling of all these elements in a single model that can be efficiently integrated numerically is one of the most relevant achievements of our work. The model describes a large variety of spatiotemporal features that can be compared with experimental realizations

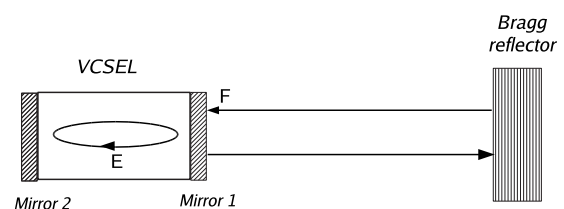


FIG. 1. Schematic of the laser with frequency-selective feedback.

<sup>\*</sup>andrew@phys.strath.ac.uk

because we do not restrict to purely temporal regimes and/or introduce restrictions in the magnitude of the feedback.

The intra-VCSEL optical field  $E$  and carrier density  $N$  are modeled using a similar description to that used for amplifier CS [6,8,9]. The holding field of the amplifier models is, however, replaced by the external cavity field at the VCSEL output mirror,  $F$ . The complete system is described by the following system of coupled partial differential equations and mapping:

$$\partial_t E = -(1 + i\theta)E + i\nabla^2 E - i\sigma(\alpha + i)(N - 1)E + \frac{2\sqrt{T_1}}{(T_1 + T_2)}F,$$

$$\partial_t N = -\gamma[N - J + |E|^2(N - 1) + D\nabla^2 N],$$

$$F(t) = e^{-i\delta\tau_f}\hat{G}(t - \tau_f/2)[-r_1 F(t - \tau_f) + t_1 E(t - \tau_f)]. \quad (1)$$

Here  $\theta$  is the detuning of the VCSEL cavity with respect to the chosen reference frequency,  $\sigma$  is a coupling constant,  $\alpha$  is the linewidth enhancement factor, and  $T_1$  and  $T_2$  are the transmittivities of the VCSEL mirrors. The parameter  $J$  represents the injection current, normalized to the value at transparency. Time is scaled to the VCSEL cavity lifetime, and  $\gamma$  is the ratio of cavity lifetime to carrier response time in the VCSEL. The term  $D\nabla^2 N$  describes carrier diffusion but will generally be omitted in what follows.

The external cavity carrier field detuning and the external round-trip time are denoted by  $\delta$  and  $\tau_f$ , respectively, while  $r_1$  and  $t_1$  are the (real) amplitude reflection and transmission coefficients of the VCSEL output mirror, (i.e.,  $T_1 = t_1^2 = 1 - r_1^2$ ; see [24] for a detailed description of the external cavity). The operator  $\hat{G}$  describes the frequency-selective operation of the Bragg reflector on the field envelope and is taken to be

$$\hat{G}(t)[h(t)] = \frac{r_g}{2\beta} \int_{t-2\beta}^t e^{i\Omega_g(t'-t)} h(t') dt' \quad (2)$$

in the time domain or, equivalently,

$$\hat{G}(\omega)[h(\omega)] = r_g e^{-i\beta(\Omega_g - \omega)} \text{sinc}[\beta(\Omega_g - \omega)] h(\omega) \quad (3)$$

in the frequency domain. The frequency  $1/\beta$  determines the bandwidth of the Bragg reflector while  $\Omega_g$  is its central frequency (henceforth referred to as the grating frequency) relative to the reference (carrier) frequency. The parameter  $r_g$  is an overall reflection coefficient. Note that in this description we neglect the transverse wave-vector dependence of the reflector response. We have also ignored transverse effects of free-space propagation (i.e., diffraction) in the external cavity since in the corresponding experiment the VCSEL output coupler is imaged directly onto the Bragg reflector [15].

This system of equations has the well-known transverse translational symmetry found in driven-cavity models. In addition, however, it has a global phase symmetry, as expected for a laser but broken by the injected field in driven cavities. Note that all variables and parameters in Eqs. (1) are dimensionless.

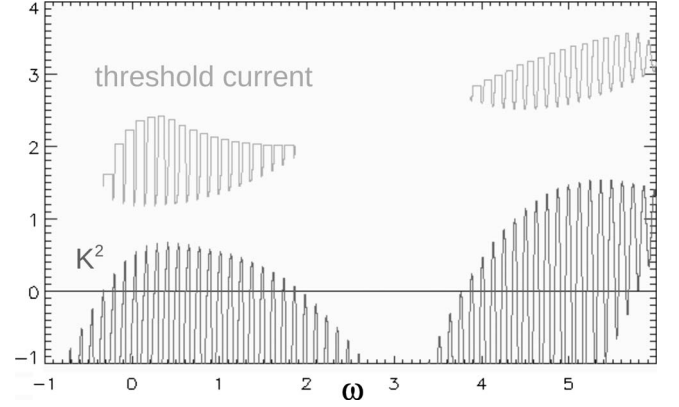


FIG. 2. Plots of threshold current (upper curve) and square of transverse wave vector (lower curve) for traveling-wave modes of the laser. Parameters:  $\alpha=5$ ,  $\theta=0$ ,  $\sigma=0.45$ ,  $\gamma=0.01$ ,  $T_1=0.008$ ,  $T_2=0.0002$ ,  $\beta=1.0$ ,  $r_g=0.9$ ,  $\delta=0$ , and  $\tau_f=50$ . The horizontal lines in the threshold current curves are artificially introduced to help delineate their upper envelopes.

### III. TRAVELING-WAVE MODES

We can calculate exact traveling-wave solutions to Eqs. (1) of the form

$$E = A e^{i(\mathbf{K}\cdot\mathbf{x} - \omega t)}, \quad F = B e^{i(\mathbf{K}\cdot\mathbf{x} - \omega t)}, \quad N = N_0 = \frac{J + |A|^2}{1 + |A|^2}. \quad (4)$$

From Eqs. (1),  $B$  satisfies

$$B = (-r_1 B + t_1 A) r_g e^{i(\omega - \delta)\tau_f} e^{-i\beta(\Omega_g - \omega)} \text{sinc}[\beta(\Omega_g - \omega)] \quad (5)$$

and therefore

$$B = \frac{r_g t_1 A e^{i\Phi} \text{sinc}[\beta(\Omega_g - \omega)]}{1 + r_g r_1 e^{i\Phi} \text{sinc}[\beta(\Omega_g - \omega)]} \equiv \frac{(T_1 + T_2)}{2\sqrt{T_1}} S(\omega) A, \quad (6)$$

where

$$\Phi = (\omega - \delta)\tau_f - \beta(\Omega_g - \omega). \quad (7)$$

From Eqs. (1) and (6), we have

$$0 = -1 + \frac{\sigma(J - 1)}{1 + |A|^2} + \text{Re}[S(\omega)], \quad (8a)$$

$$f(\omega) \equiv \omega - \alpha - \theta + \alpha \text{Re}[S(\omega)] + \text{Im}[S(\omega)] = K^2. \quad (8b)$$

Thus, values of  $\omega$  for which  $f(\omega) \geq 0$  correspond to possible modes of the system. Since  $f(\omega)$  is independent of injection

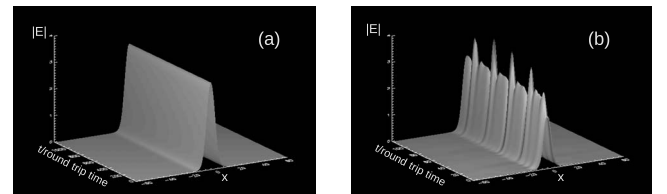


FIG. 3. Space-time plots of 1D solitons. External cavity round-trip time is (a) 5 VCSEL cavity lifetimes (b) 50 VCSEL cavity lifetimes. Other parameters as in Fig. 2 with  $J=2.45$ .

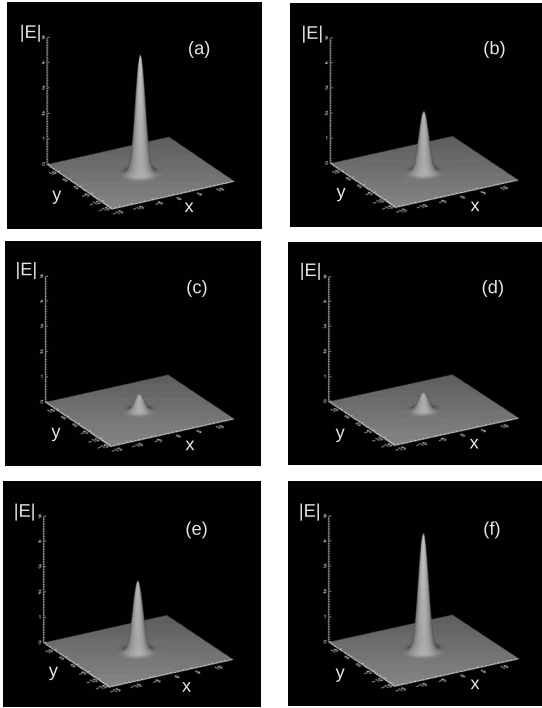


FIG. 4. Time sequence of an oscillating 2D soliton. Parameters:  $\alpha=9$ ,  $\theta=-1$ ,  $\sigma=0.9$ ,  $\gamma=0.01$ ,  $T_1=0.008$ ,  $T_2=0.0002$ ,  $\beta=1.0$ ,  $r_g=0.9$ ,  $\delta=0.832$ , and  $\tau_f=5$ . (a)  $t=0$ , (b)  $t=2.5$ , (c)  $t=3.5$ , (d)  $t=4.0$ , (e)  $t=5.0$ , and (f)  $t=7.0$  VCSEL cavity lifetimes.

current  $J$ , the modal amplitude for any current value, at a given frequency, is obtained by solving Eq. (8a).

An example of the laser modal spectrum is given in Fig. 2, along with the corresponding mode thresholds. The small-scale oscillations in Fig. 2 reflect the narrow mode spacing of the external cavity, while the larger-scale modulation is due to the response of the Bragg reflector. There is clearly a set of modes grouped around the grating frequency ( $\omega=0$ ) and other modes coming into play around the solitary VCSEL lasing frequency ( $\omega=5$ ), with a frequency gap in between. The former modes owe their existence to the strong feedback provided by the grating in the region of  $\omega=0$  and, as a result, have the lowest thresholds. The latter modes exist where the feedback is small and so can be termed VCSEL modes, although the influence of the external cavity is still apparent.

The separation of grating-determined modes and VCSEL modes is accomplished through adjustment of the detuning between VCSEL and grating frequencies (and of other system parameters). Suitable operating conditions will also create a threshold gap between the highest-threshold grating mode and the lowest-threshold VCSEL mode (Fig. 2). As a result, a range of currents opens up where the grating-determined modes exist (i.e., the system can lase) but where the laser off state is also stable (i.e., the system can also not lase). In this region there is therefore bistability between lasing and nonlasing states, and the possibility of observing localized lasing on a zero-field background: in other words, laser cavity solitons [15,16].

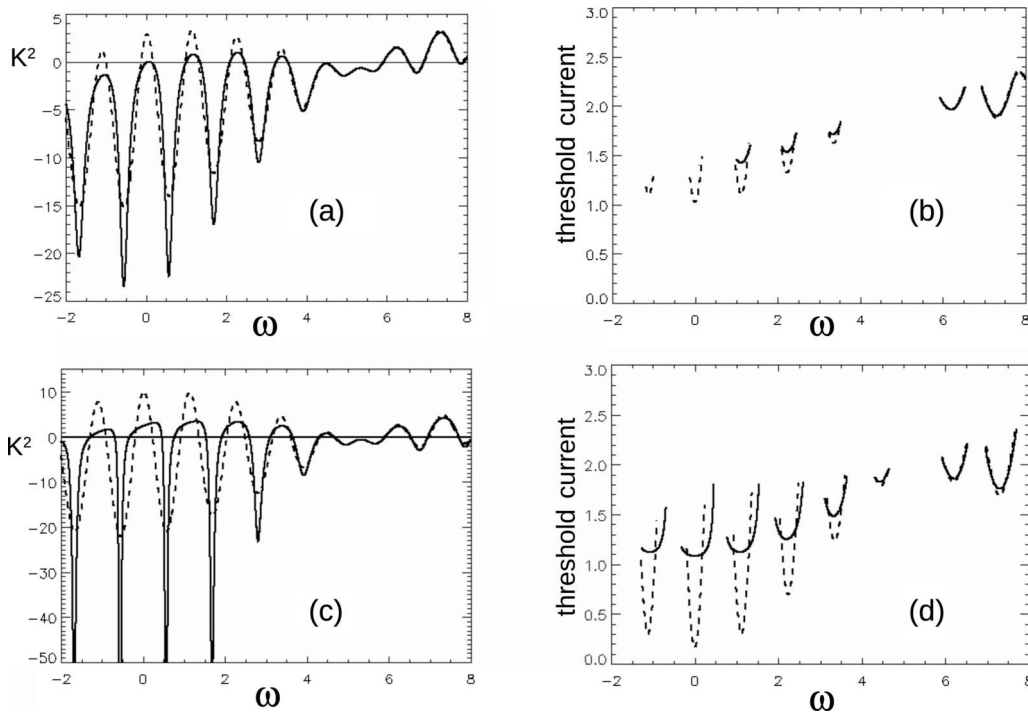


FIG. 5. Comparison between external-cavity (solid line) and Lang-Kobayashi (dashed line) models in the vicinity of the grating frequency ( $\omega=0$ ). (a) and (c) Plane-wave modes  $K^2(\omega)$  for the laser with feedback, for  $r_g=0.5$  and  $r_g=0.9$ , respectively. Only portions of each curve above the line  $K^2=0$  are physically relevant. (c) and (d) Threshold current versus  $\omega$  for the modes in (a) and (c), respectively. Gaps in the threshold curves correspond to intervals where  $K^2(\omega) < 0$ . (d) depicts threshold currents below the transparency value of  $J=1$  for the LK approximation, indicating lasing even when the laser medium is not amplifying. Parameters:  $\alpha=9$ ,  $\theta=-3$ ,  $\sigma=0.9$ ,  $\gamma=0.01$ ,  $T_1=0.008$ ,  $T_2=0.0002$ ,  $\beta=1.0$ ,  $\delta=0$ , and  $\tau_f=50$ .

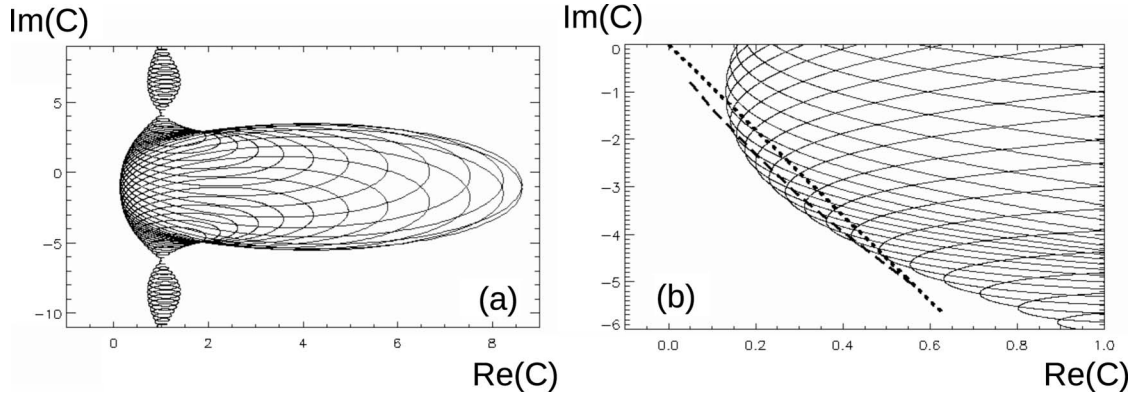


FIG. 6. (a) Effective cavity response [Eq. (10a)] for the coupled-cavity system plotted in the complex  $C$  plane. (b) Blowup of (a) showing the soliton (dashed line) for a current  $J=1.63$  and plane-wave threshold (dotted line) solutions of Eq. (10a). All soliton solution curves terminate on the threshold line in the limit where soliton amplitude tends to zero and width tends to infinity. Parameters:  $\alpha=9$ ,  $\theta=-1$ ,  $\sigma=0.9$ ,  $\gamma=0.01$ ,  $T_1=0.008$ ,  $T_2=0.0002$ ,  $\beta=0.6$ ,  $r_g=0.8$ ,  $\delta=0$ , and  $\tau_f=20$ .

Numerical integration of Eqs. (1) verifies that laser solitons can indeed be initiated in the current gap. As Figs. 3 and 4 show, the soliton can be either single or multifrequency, depending on system parameters. This issue will be discussed in more detail in Sec. VII below.

#### IV. HIGH REFLECTIVITY OF THE FEEDBACK MIRROR

In this section we briefly comment on the advantages of the full external-cavity model [Eqs. (1)] that extends to high-reflectivity feedback mirrors, compared to the more common Lang-Kobayashi (LK) approximation for modeling lasers with external feedback (see, e.g., [17–23]). In the latter, the effects of multiple round trips in the external cavity are neglected, giving rise to a VCSEL feedback field which is simply a scaled delayed version of the VCSEL output. This can be justified only if the external cavity finesse is sufficiently small to neglect multiple-interference effects. The model given by Eqs. (1) describes operational regimes of CS lasers with arbitrarily high reflectivities of the frequency-selective feedback mirror [25]. It also recovers the LK approximation by setting the VCSEL external reflection coefficient  $r_1$  to zero, thus, allowing for a quantitative comparison.

Figure 5 compares the external cavity and LK models for two different external cavity finesses, controlled by altering the reflection coefficient  $r_g$  of the external Bragg reflector. Figures 5(a)–5(d) show that there are some quantitative and qualitative differences which become more pronounced as  $r_g$  is increased. This is not unexpected. The key point, however, is illustrated in Figs. 5(b) and 5(d) which plot the threshold current as a function of frequency. For an external reflectivity as low as 0.25, the laser threshold current in the LK model is almost equal to the transparency current ( $J=1$ ). For an external reflectivity of 0.81, which corresponds approximately to experimental conditions [25], the LK laser threshold is well below transparency, indicating that lasing is predicted to occur even without a population inversion, which is unphysical.

The source of the problem lies in the failure of the LK approximation to conserve energy through its one-sided ne-

glect of the reflectivity of the VCSEL output coupler. As examination of Eqs. (1) shows, this can lead to a feedback strength which exceeds the VCSEL cavity losses, and hence to unphysical linear gain even when the laser gain medium is absorbing rather than amplifying. Numerical simulation of the system under these conditions does indeed lead to rapid blowup of the optical field  $E$ .

In contrast, a more physical treatment of the feedback loop as a true optical cavity [24] avoids this problem by observing the boundary conditions and conserving energy at the VCSEL output coupler. Moreover, this regularization is accomplished with essentially no computational overhead [24]. As Eqs. (1) show, only one extra addition and multiplication are required per time step with respect to the LK approximation, while the storage requirements for fields at earlier times are the same in both LK and external-cavity approaches. We note that this last point is made in [24] but we take this opportunity to re-emphasize it here.

We note that the LK approximation presents no blowup problem as long as the feedback term cannot exceed the VCSEL losses. Even at small values of external reflectivity,

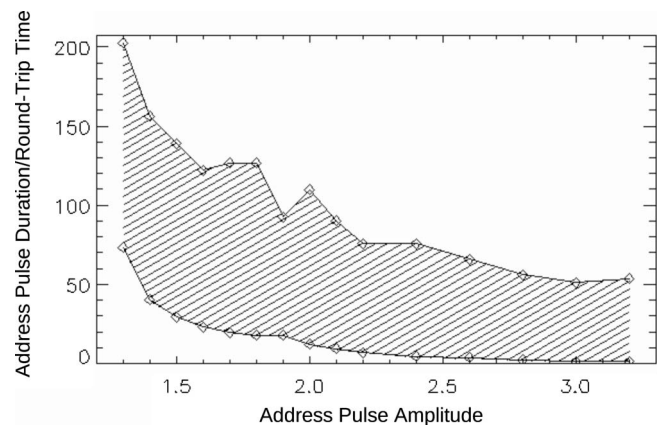


FIG. 7. Soliton creation by means of a localized finite-duration address pulse: address pulse duration versus amplitude. The shaded area represents the region of systematic soliton creation. Parameters as in Fig. 6 with  $\tau_f=41$ ,  $\eta=5$ , and  $\omega_p=0$ .

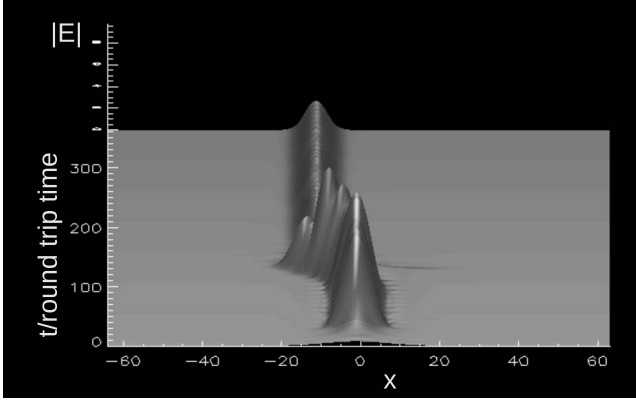


FIG. 8. Soliton migration away from center of an address pulse during switch on. Parameters as in Fig. 7 with  $P_0=1.8$ ,  $\tau_p=5400$ .

however, some rescaling of the feedback strength parameter is required, which complicates the relation between the predictions of the LK approach and the operation of real laser systems.

## V. SINGLE-FREQUENCY SOLITONS

In this section we describe some properties of single-frequency laser solitons in order to build a framework for understanding more complicated behavior. We also restrict ourselves to one transverse spatial dimension for the moment. We therefore look for solutions of the form  $E(x,t) = A(x)\exp(-i\omega t)$ .

From Eqs. (1) and (6),  $A(x)$  satisfies

$$[-i\omega + (1 + i\theta) - S(\omega)]A = i\nabla^2 A + \frac{\sigma(J-1)(1-i\alpha)}{1+|A|^2}A. \quad (9)$$

Equation (9) has been written in such a way that the left-hand side contains all frequency-dependent terms, while the right-hand side is independent of frequency and of the details of the external and VCSEL cavity properties. Equation (9) can therefore be separated into two equations,

$$[-i\omega + (1 + i\theta) - S(\omega)]A = CA, \quad (10a)$$

$$i\nabla^2 A + \frac{\sigma(J-1)(1-i\alpha)}{1+|A|^2}A = CA, \quad (10b)$$

whose simultaneous solutions correspond to single-frequency states of our laser system. Equation (10a) describes the effective cavity response and can be represented by a curve in the complex  $C$  plane parametrized by  $\omega$ . Equation (10b) represents a nonlinear eigenvalue problem for soliton solutions in which the complex parameter  $C$  corresponds to an effective loss and detuning. For a given set of parameters we can expect bounded solutions only on a null set in the complex  $C$  plane, i.e., a curve at most.

Figure 6 plots the cavity response Eq. (10a) in the complex  $C$  plane for a particular set of parameters. Traversing a loop of this curve corresponds to a phase change of  $2\pi$  in the

cavity response and hence each loop contains one cavity mode. The regions of large excursion are due to the strong response of the cavity near the grating frequency. Superimposed on this curve is a line of soliton solutions to Eq. (10b) for  $J=1.63$ , obtained by means of a shooting method [26]. As this curve is followed from left to right, the corresponding solutions become broader with lower peak amplitude. It eventually terminates, with infinite width and zero amplitude, on the straight line  $C = \sigma(J-1)(1-i\alpha)$ , parametrized by current, defining low-amplitude spatially homogeneous solutions to Eq. (10b).

Figure 6 shows that there can be many intersections between the cavity response and soliton solution curves, and hence many single-frequency soliton solutions. Moreover, it can be seen that changing a system parameter will alter the soliton and cavity response curves, creating (or destroying) laser solitons in pairs through saddle-node bifurcations (at least one of such a pair is necessarily unstable). Since  $\text{Re}(C)$  represents the net cavity loss we expect the system to favor the soliton which minimizes this quantity. Numerical simulation bears this out: as new solitons appear on changing a system parameter, the laser has a tendency to shift operation to the soliton with the smallest losses. We elaborate on this in the next section.

## VI. ADDRESSING OF LASER SOLITONS

In this section we discuss some features of the creation of solitons in the coupled-cavity laser. Our simulations mimic experimental procedure [15,16,25] by initiating a soliton through the application of a spatially-localized rectangular address pulse  $P(x,t)$  of the form

$$P(x,t) = P_0 \exp\left(-\frac{x^2}{\eta^2} - i\omega_p t\right) \text{rect}\left(\frac{t}{\tau_p}\right). \quad (11)$$

Computationally, the amplitude, width, duration, and frequency of the address pulse can all be altered.

Fixing the width and frequency of the address pulse allows us to map a region of successful soliton initiation in the plane of the remaining two parameters. In Fig. 7 solitons can be systematically created in the shaded region between the lower and upper curves. Below the lower curve, the address pulse is either too short or of too low amplitude to succeed in dragging the system from the off state into the basin of attraction of the soliton before the pulse is switched off. It can be seen that there is an unsurprising tradeoff between address pulse amplitude and duration. It should also be noted that there is an apparent vertical asymptote at the left-hand side of the curve, for a pump amplitude somewhere between 1.2 and 1.3. This indicates that a minimum peak address power is required, irrespective of pulse duration.

Above the upper boundary of the shaded region in Fig. 7, the system appears to overshoot the soliton. The sustained application of a high-power address pulse drives the system strongly so that when the address pulse is removed, the system can relax either to a soliton or to the off state in a way

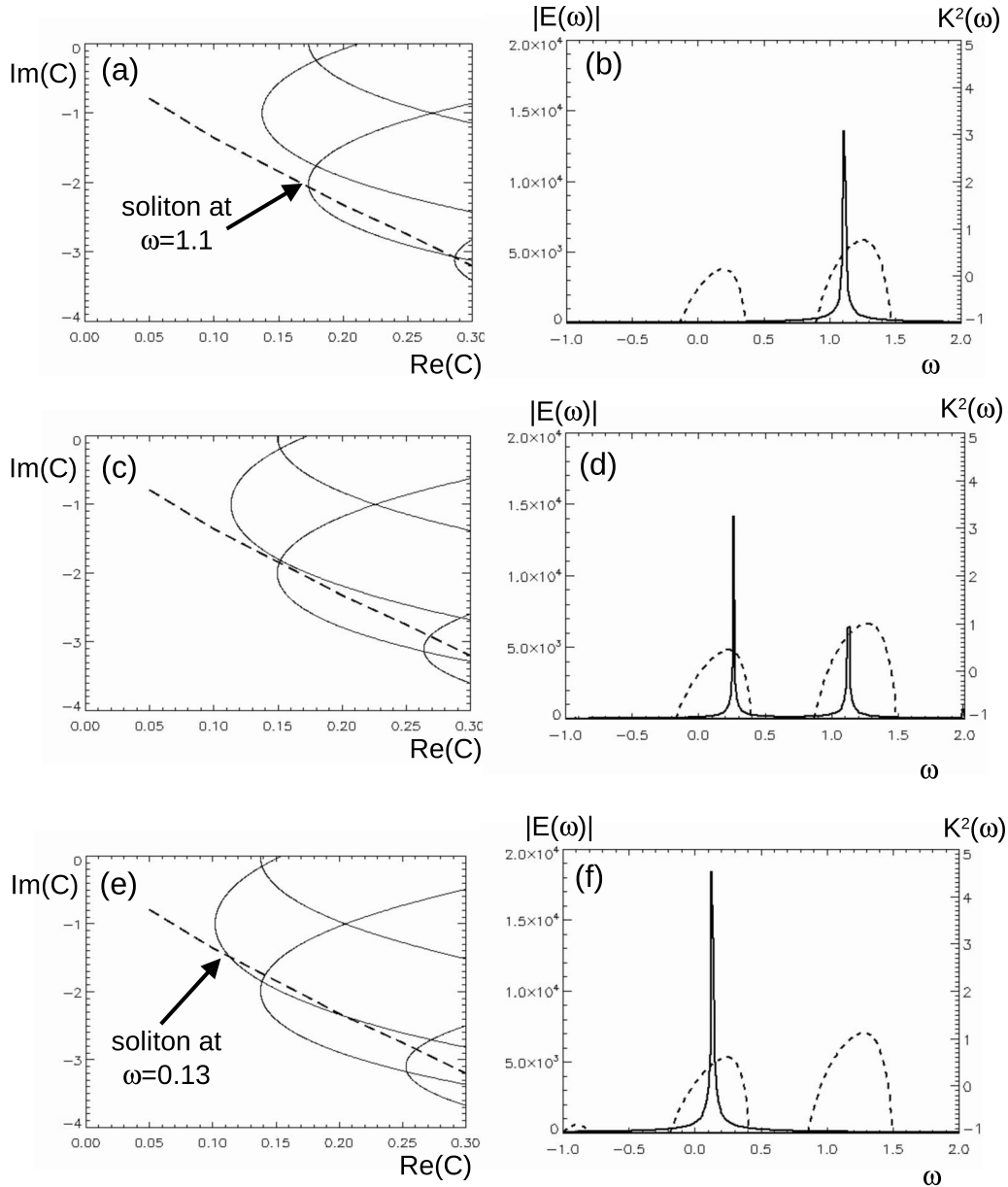


FIG. 9. Birth of new soliton pair on changing the feedback reflectivity  $r_g$ . (a), (c), and (e) Cavity response curve (solid curves) and soliton solution curve (dashed curves) in the complex  $C$  plane. (b), (d), and (f) Corresponding spectra (solid curves) and traveling-wave transverse wave-vectors (dashed curves). (a) and (b)  $r_g=0.79$ . (c) and (d)  $r_g=0.83$ . (e) and (f)  $r_g=0.85$ . Other parameters as in Fig. 6 except  $\tau_f=5$ .

that is essentially unpredictable. The strongly nonlinear dynamics can also lead to migration of the induced structure from the center of the address pulse to a location where it is apparently more easily sustained, as in Fig. 8. Moreover, successful soliton switching can recur in intervals above the upper curve in Fig. 7 (not shown). All of these features render the upper threshold inherently more difficult to delineate, and so the curve in Fig. 7 should be seen as a guide rather than a firm boundary.

In summary, the shaded area in Fig. 7 represents the region of parameter space in which successful soliton switching can be reliably predicted. We expect the qualitative features of Fig. 7 to be generic for lasers with FSF.

## VII. SIDEBAND INSTABILITIES AND MULTIFREQUENCY LASING

As mentioned above, virtually any system parameter can be used to bring new single-frequency solitons into existence. Here we select the reflection coefficient  $r_g$  of the Bragg grating as our unfolding parameter. We also choose to analyze a system with shorter external cavity (round-trip time  $\tau_f=5$ ) than in Fig. 6. This increases the external-cavity mode spacing, decreases the density of loops in the cavity response curve [Eq. (10a)], and makes it easier to observe the birth of new soliton solutions.

For  $r_g=0.79$ , Fig. 9(a) shows a section of the complex  $C$  plane indicating an intersection between soliton and cavity-

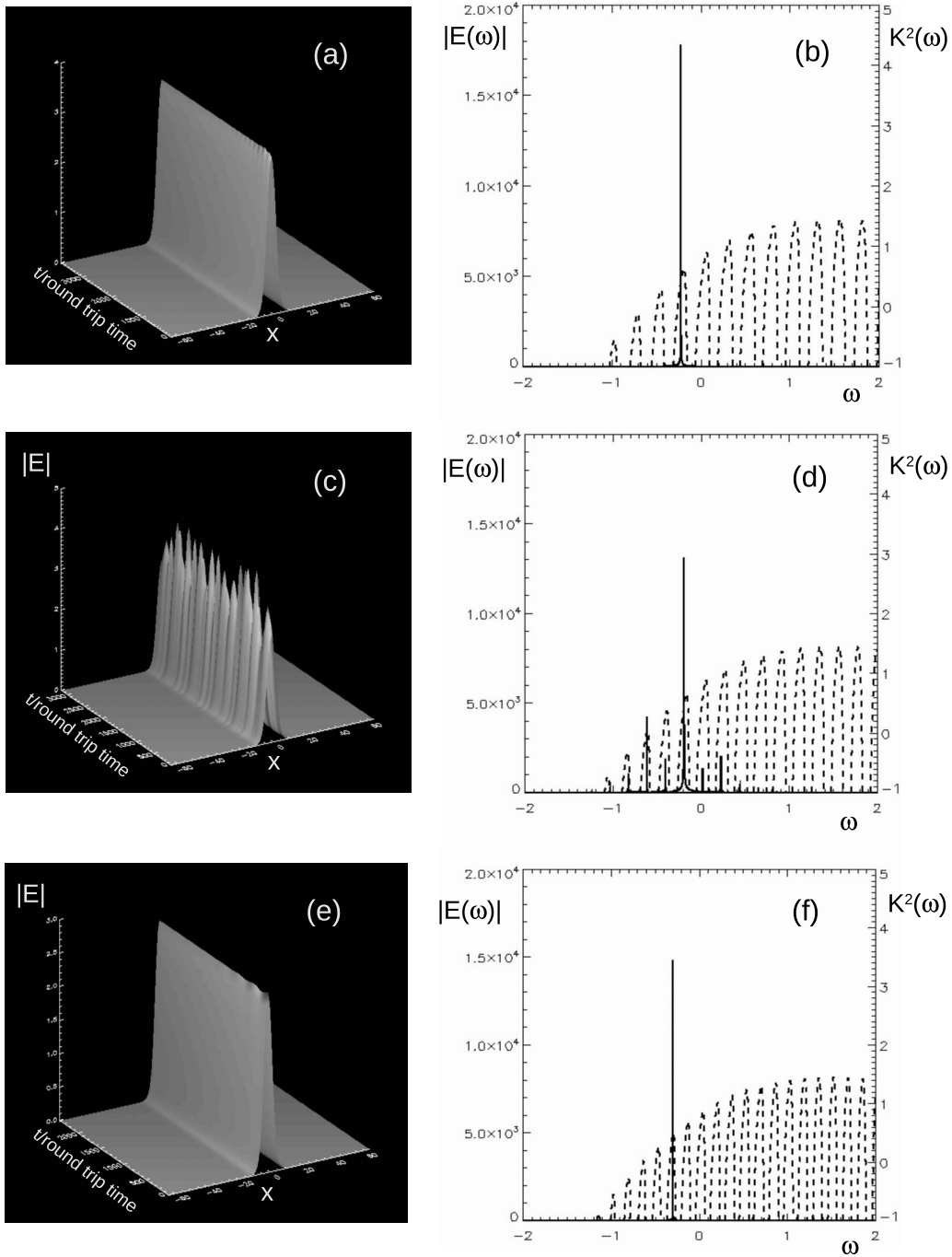


FIG. 10. Appearance and disappearance of CS sideband instability on increasing external cavity length. (a), (c), and (e) Space-time plots of the soliton. (b), (d), and (f) Corresponding spectra (solid curves) and traveling-wave transverse wave vectors (dashed curves). (a) and (b)  $\tau_f=24$ . (c) and (d)  $\tau_f=28$ . (e) and (f)  $\tau_f=37$ . Other parameters as in Fig. 6.

response curves at a frequency  $\omega \approx 1.1$ . Figure 9(b) shows the soliton spectrum obtained from a numerical simulation of Eqs. (1) for these parameters. The soliton is initiated by means of an address pulse at the grating frequency ( $\omega=0$ ) and the system allowed to relax to its preferred state. The spectrum in Fig. 9(b) is that of the central point of the soliton and can be seen to correspond to the predicted soliton frequency at  $\omega \approx 1.1$ . Also shown for context in Fig. 9(b) is the (inverse) dispersion curve  $K^2(\omega)$  (cf. Fig. 2). Note the exist-

tence of other solitons at higher values of  $\text{Re}(C)$  but that the system selects the one with smallest losses.

Figure 9(e) shows that when  $r_g=0.85$  a new soliton has appeared with  $\omega \approx 0.13$ . Numerical integration [Fig. 9(f)] using the previous soliton as initial condition confirms that the system now selects the new soliton, which has a frequency closer to the grating frequency and therefore sees even smaller losses. As Fig. 9(f) shows, the new soliton appears in the band of modes adjacent to that containing the original

soliton, consistent with the fact that the new intersection in Fig. 9(e) occurs on the next loop of the cavity-response curve.

However, in an interval between these two values (e.g.,  $r_g=0.83$ ) the laser soliton contains frequencies corresponding to those of the two single-frequency solitons on either side [Fig. 9(d)]. This is true even before the new lower-frequency soliton has come into existence [Fig. 9(c)] and this behavior therefore acts as a precursor to a switch in laser operation between different frequency bands.

This phenomenology appears to be quite general and analogous to what happens in a laser with transverse modes when changing the cavity length [27], although single-transverse-mode solutions correspond here to single-frequency solitons. Increasing the cavity round trip time will generate a sideband instability of a single-frequency soliton followed by the eventual appearance of a new single-frequency soliton in an adjacent band (Figs. 10 and 3). In these simulations we have assumed that the external cavity is in resonance ( $\delta=0$ ) for  $\tau_f=1$  and hence for any whole value of  $\tau_f$ .

There is, however, an interesting feature of using  $\tau_f$  as a control parameter in this way: namely, that for a given frequency, the feedback term in Eq. (6) is periodic in  $\tau_f$ . This means that if a CS appears with frequency  $\omega_0$  via a saddle-node bifurcation at  $\tau_f=\tau_{f0}$ , there will be an infinite sequence of such bifurcations for  $\tau_f=\tau_{f0}+2n\pi/\omega_o$ , where  $n$  is an integer. Each new soliton will appear with the same frequency  $\omega_0$  and the same amplitude. This periodic behavior with changing external cavity length is analogous to the periodicity of the spectrum of a scanning Fabry-Pérot resonator.

Of course the periodicity which applies to  $\omega_0$  does not apply to other frequencies, and the dynamical instabilities of these soliton branches may be quite different. On increasing  $\tau_f$ , we observe the system's preference to switch to a newly created soliton solution in an adjacent band of modes, as when the external reflectivity is varied. However, we also observe a tendency toward a larger number of frequencies in the transition region between single-frequency behavior, and to such complicated dynamics that it is very difficult (or even apparently impossible) to initiate a soliton for certain ranges of external cavity length. This makes single-frequency operation, and indeed any form of soliton at all, increasingly difficult to observe as the external cavity is lengthened. A useful corollary is that in the limit in which the external cavity length goes to zero, the system dynamics become simpler and the laser goes inevitably toward single-frequency behavior. Note that a similar periodicity exists with respect to the external cavity detuning  $\delta$  (see, for example, Fig. 4) and also that in practice these two quantities ( $\delta$  and  $\omega_0$ ) should be connected to each other.

## VIII. CONCLUSION

We have constructed a model of a VCSEL with external frequency-selective feedback and shown that it captures physical features of the corresponding experiment essential for cavity soliton formation. Our coupled-cavity approach is capable of describing regimes of CS laser operation with arbitrary reflectivity of the frequency-selective feedback mirror, thus, improving on the more common Lang-Kobayashi approximation.

The solitons produced in the laser can be either single frequency (stationary in intensity) or multiple frequency (oscillating intensity), involving several cavity modes. Investigation of single-frequency solutions through a separation of cavity and intrinsic effects provides some insight into this phenomenon, as well as providing a framework in which the effects of different cavities can be assessed with only trivial re-computation. Our analysis points toward the fact that single-frequency behavior occurs in the limit of zero external cavity length. This result is useful and promising for integrated devices.

Because of the time delay involved in the feedback mechanism, the optical addressing of laser solitons is non-trivial. The address beam must be sufficiently sustained or sufficiently intense to overcome the delay and decay involved in establishing the feedback required to support lasing. In addition, a minimum peak power seems necessary. The minimum threshold curve shown in Fig. 7 is experimentally accessible and should provide a useful qualitative comparison with the present model.

The laser with frequency-selective feedback has shown itself to be a promising candidate for a practical transverse soliton laser. When compared with other cavity soliton lasers based either on saturable absorbers [13], coupled cavities [14], or optical injection [11], VCSELs with FSF present a high degree of stability of soliton operation and simplicity of construction. The model described here captures the essential features of the CS laser with FSF and demonstrates the wide range of existence, stability, and application of laser CS in this device. It also provides evidence of the dynamical properties of laser CS operation with possible applications in the storage and processing of optical information.

## ACKNOWLEDGMENTS

We acknowledge useful discussions with T. Ackemann and N. Radwell. This work was supported by the EU FET Open FunFACS.

- 
- [1] *Dissipative Solitons*, edited by N. Akhmediev and A. Ankiewicz, Lecture Notes in Physics Vol. 661 (Springer, New York, 2005).  
 [2] W. J. Firth *et al.*, *J. Opt. Soc. Am. B* **19**, 747 (2002).

- [3] W. J. Firth and A. J. Scroggie, *Phys. Rev. Lett.* **76**, 1623 (1996).  
 [4] V. B. Taranenko and C. O. Weiss, *Appl. Phys. B: Lasers Opt.* **72**, 893 (2001).

- [5] G.-L. Oppo, A. J. Scroggie, and W. J. Firth, *J. Opt. B* **1**, 133 (1999).
- [6] S. Barland *et al.*, *Nature (London)* **419**, 699 (2002).
- [7] S. Barbay *et al.*, *Opt. Lett.* **31**, 1504 (2006).
- [8] L. Spinelli, G. Tissoni, M. Brambilla, F. Prati, and L. A. Lugiato, *Phys. Rev. A* **58**, 2542 (1998).
- [9] F. Pedaci *et al.*, *Appl. Phys. Lett.* **92**, 011101 (2008).
- [10] Y. Larionova and C. Weiss, *Opt. Express* **13**, 10711 (2005).
- [11] X. Hachair *et al.*, *IEEE J. Sel. Top. Quantum Electron.* **12**, 339 (2006).
- [12] V. B. Taranenko, K. Staliunas, and C. O. Weiss, *Phys. Rev. A* **56**, 1582 (1997).
- [13] M. Bache *et al.*, *Appl. Phys. B: Lasers Opt.* **81**, 913 (2005).
- [14] P. Genevet, S. Barland, M. Giudici, and J. R. Tredicce, *Phys. Rev. Lett.* **101**, 123905 (2008).
- [15] Y. Tanguy, T. Ackemann, W. J. Firth, and R. Jäger, *Phys. Rev. Lett.* **100**, 013907 (2008).
- [16] Y. Tanguy, N. Radwell, T. Ackemann, and R. Jäger, *Phys. Rev. A* **78**, 023810 (2008).
- [17] *Unlocking Dynamical Diversity: Optical Feedback Effects on Semiconductor Lasers*, edited by D. M. Kane and K. A. Shore (Wiley, New York, 2005).
- [18] P. V. Paulau, A. J. Scroggie, A. Naumenko, T. Ackemann, N. A. Loiko, and W. J. Firth, *Phys. Rev. E* **75**, 056208 (2007).
- [19] P. V. Paulau, D. Gomila, T. Ackemann, N. A. Loiko, and W. J. Firth, *Phys. Rev. E* **78**, 016212 (2008).
- [20] R. Lang and K. Kobayashi, *IEEE J. Quantum Electron.* **16**, 347 (1980).
- [21] G. H. M. van Tartwijk and D. Lenstra, *Quantum Semiclass. Opt.* **7**, 87 (1995).
- [22] D. Pieroux and P. Mandel, *Phys. Rev. E* **68**, 036204 (2003).
- [23] M. Yousefi, D. Lenstra, and G. Vemuri, *Phys. Rev. E* **67**, 046213 (2003).
- [24] M. Giudici *et al.*, *J. Opt. Soc. Am. B* **16**, 2114 (1999).
- [25] N. Radwell, Y. Tanguy, and T. Ackemann, *IEEE J. Quantum Electron.* (to be published).
- [26] W. H. Press *et al.*, *Numerical Recipes*, 3rd ed. (Cambridge University Press, Cambridge, 2007).
- [27] L. A. Lugiato *et al.*, *J. Opt. Soc. Am. B* **7**, 1019 (1990).